

This is an Open Access document downloaded from ORCA, Cardiff University's institutional repository: <https://orca.cardiff.ac.uk/id/eprint/115822/>

This is the author's version of a work that was submitted to / accepted for publication.

Citation for final published version:

Smith, Paul J., Darzynkiewicz, Zbigniew and Errington, Rachel J. 2018. Nuclear cytometry and chromatin organization. *Cytometry Part A* 93 (8) , pp. 771-784. 10.1002/cyto.a.23521

Publishers page: <http://dx.doi.org/10.1002/cyto.a.23521>

Please note:

Changes made as a result of publishing processes such as copy-editing, formatting and page numbers may not be reflected in this version. For the definitive version of this publication, please refer to the published source. You are advised to consult the publisher's version if you wish to cite this paper.

This version is being made available in accordance with publisher policies. See <http://orca.cf.ac.uk/policies.html> for usage policies. Copyright and moral rights for publications made available in ORCA are retained by the copyright holders.



Nuclear Cytometry and Chromatin Organisation

Paul J Smith¹, Zbigniew Darzynkiewicz² and Rachel J Errington¹

¹Division of Cancer and Genetics, School of Medicine, Tenovus Building, Cardiff University, Heath Park, Cardiff, CF14 4XN, United Kingdom. ²Department of Pathology, Brander Cancer Research Institute, New York Medical College, Valhalla, New York 10595, USA.

Running headline: Chromatin & Probes

Correspondence: smithpj2@cf.ac.uk

Division of Cancer and Genetics

School of Medicine, Tenovus Building

Cardiff University

Heath Park, Cardiff

CF14 4XN, United Kingdom

Tel: +44 (0)29 206 87301

Key Words

DNA Topology

Chromatin

Histones

Nucleosomes

DNA Dyes

DNA Targeted Drugs

DNA Damage

DNA Topoisomerases

Electron Microscopy

Super Resolution Microscopy

Abbreviations

SAF-A: scaffold attachment factor A

HMM: Hidden Markov Model

FLIM: Fluorescence Lifetime Imaging Microscopy SIM: Saturated Structured Illumination Microscopy

STED: Stimulated Emission Depletion

STORM: Stochastic Optical Reconstruction Microscopy

PALM: Photoactivation Localization Microscopy

fPALM fluorescence-based PALM

SMLM: Single Molecule Localization Microscopy

SPDM: Spectral Precision Distance/Position Determination Microscopy

BALM: Binding-Activated Localization Microscopy

DAB: diaminobenzidine

ROS: Reactive Oxygen Species

DAPI: (4',6-Diamidino-2- phenylindole dihydrochloride)

IdU: 5-iodo-2-deoxyuridine

AO: Acridine Orange

CARS: Coherent anti-Stokes Raman scattering

MSI: Mass Spectrometry Imaging

PWS: Partial-wave spectroscopic

MTG: MitoTracker Green

ERTG: Endoplasmic Reticulum Tracker Green

NETs: Neutrophil Extracellular Traps

m-AMSA: 4'-(9-acridinylamino) methane sulfon-m-anisidine

MTX: mitoxantrone

μPK-PD-CD: Micro-PharmacoKinetics and cellular PharmacoDynamics with specific Cellular Descriptors

Abstract:

The nuclear-targeting chemical probe, for the detection and quantification of DNA within cells, has been a mainstay of cytometry - from the colorimetric Feulgen stain to smart fluorescent agents with tuned functionality. The level of nuclear structure and function at which the probe aims to readout, or indeed at which a DNA-targeted drug acts, is shadowed by a wide range of detection modalities and analytical methods. These methods are invariably limited in terms of the resolution attainable

versus the volume occupied by targeted chromatin structures. The scalar challenge arises from the need to understand the extent and different levels of compaction of genomic DNA and how such structures can be re-modelled, reported or even perturbed by both probes and drugs. New cytometric approaches to analysing chromatin released from cells, as in NETosis, demonstrate the potential for probes to report defining features. Typical of recent insights into chromatin organisation is the 'ChromEMT' study that exploits the properties of the anthraquinone-based cytometric dye DRAQ5™. Insights reveals that local and global 3D chromatin structures in the nucleus determine compaction. Cytometry can report on complex levels of chromatin order, disorder, disassembly and active disruption. The focus of this review is nuclear cytometry, with linked reference to DNA targeting drugs and probes, their impact in the chromatin environment.

Introduction

‘form ever follows function’

Louis Henry Sullivan (1856 – 1924)

American architect and ‘father of skyscrapers’

Cellular structures, first recognised by von Nägeli in 1842, would later be called ‘chromosomes’ by Waldeyer in 1888 to reflect their staining behaviour with dyes. The observable packaging of a cell’s genetic material and its metrology have provided a continuing source of interest through to modern cytogenetics. Cytometry in its widest definition has a considerable track record in the analysis of the multi-level organisation of the genetic material in eukaryotic nuclei (1-8). Nuclear cytometry-based methods can simplify the analysis and quantification of protein associations to chromatin and reveal population heterogeneity (9). Recent methods describe the extraction of nuclei for the purpose of probing cellular and transcriptional states (10,11) although preserving native chromatin superstructure remains a challenge. Extensive information is available from academic and commercial sources on the spectral properties of molecular probes for nuclear cytometry that can report nuclear states. This review will not explore these in detail. However, understanding the balance of advantages and limitations is important when a given probe is used for specific purposes or in a sensitive cellular system (12,13). Critical factors in live cell studies are the biological impact of the probe and its access to a nuclear target determined by chromatin organisation (14). Such factors are shared by nuclear-targeted drugs in driving their pharmacodynamic effects. Here these aspects are discussed with respect to DNA-interactive probes, with linked reference to DNA targeting drugs, in the context of the chromatin environment.

Chromatin organisation

Genomic DNA is compacted into chromatin through packaging with histone and non-histone proteins. Chromatin folding and packaging has to change dynamically as the cell progresses through the cell cycle. Chromatin organisation is addressable by DNA-affinic probes. The challenge is how to recognise and measure different scalar levels of chromatin organisation, from base-pair to the whole nucleus. The scalar levels of chromatin organisation dictate the analytical approach employed and the extent to which a probe can be usefully deployed (Fig. 1). The cell deals with an impressive length of linear DNA packaged within its nuclear volume. Towards one end of the scale, haploid yeast cells with a mean nuclear volume of $3 \mu\text{m}^3$ has a genome length of $\sim 12 \text{ Mbp}$. This represents some 0.3 % of the nuclear volume or around $0.01 \mu\text{m}^3$. A human diploid cell nucleus with a volume of around $700 \mu\text{m}^3$ copes with 3 billion bases and a combined strand length of genomic DNA of just over 2 m.

There is increasing evidence of a relationship between higher orders of chromatin topology and the regulation of global patterns of gene expression (15). One concept is that evolutionary selection favours the clustering of widely expressed housekeeping genes. Such clusters adopt an open configuration of chromatin structure. Open chromatin fibres have also been found to be enriched in

gene-rich domains and not just in those regions that are transcriptionally active (16). The mechanisms by which large-scale chromatin structures can be de-compacted or undergo dynamic folding are becoming clearer (17). An informative example is how the scaffold attachment factor A (SAF-A) can interact with chromatin-associated RNAs in a transcription-dependent manner. SAF-A oligomerization de-compacts large-scale chromatin structure while SAF-A loss or monomerization promotes aberrant chromosome folding and the accumulation of genome damage (17). This also highlights a crucial role for chromatin organisation in maintaining a stable environment for the genome.

Annotation of the human genome with respect to different chromatin states can reveal signatures for functional descriptions. Descriptors can reflect transcription-associated or active large-scale repressed states (18). Recently the ChromHMM tool has been described that can seek signatures of chromatin-states using a multivariate hidden Markov model (HMM) (19). The tool performs an enrichment analysis of the resulting annotations to allow functional interpretation (19). Advances in the high-resolution approaches of electron and super-resolution fluorescence microscopy, together with DNA sequencing, have provide views of the relationship between chromatin and nuclear machineries within a '4D nucleome' (20). This approach has provided a finer structural definition of active and inactive nuclear compartments. An inactive compartment comprises the core of chromatin domain clusters. The active compartment locates at the periphery of these clusters. A further compartment links to routes for nuclear import and export via nuclear pores (20).

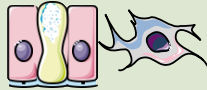


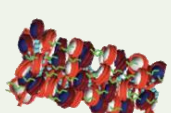

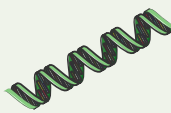
Analysis level	DNA analysis scale level	Detection ranges for exemplar methods	Molecular probe & reporter deployment
	micro-community to single cell [2000-20 μm]	<i>tissue histopathology, flow/image/mass cytometry; Raman scattering; incorporation methods; photoacoustics</i>	Cell recognition, location, tracking & status, differentiation, viability & function
	nucleus & cell cycle dynamics [20-1 μm]	<i>live and fixed cell fluorescent reporters,</i>	Nuclear structure and state changes, functional distributions, kinetics, targeting
	sub-chromosomal regions [2-0.1 μm]	<i>Super Resolution Optical Microscopy Opto-methods (eg FRET) ChromEMT</i>	Banding, telomere, centromere structural changes; high resolution signal location & relationships
	chromatin fibre & packing [30-10 nm]	<i>atomic force microscopy imaging electron microscopy phase plate cryo-EM imaging electron spectroscopic imaging</i>	Chromatin compaction; dynamic changes and perturbation
	nucleosome & protein binding [6 nm]	<i>Structural approaches: nuclear magnetic resonance spectroscopy,</i>	DNA metabolism, winding and unwinding dynamics; receptor binding
	duplex DNA & sequence/groove interactions [10bp: 2.4 x 3.4 nm]	<i>X-ray crystallography</i>	Sequence selectivity and structural modification, damage & repair; ligand binding

Figure 1: Probing the hierarchy of chromatin organization

At its lowest level, DNA wraps around histone octamers to form nucleosomes but needs to eventually compact into discrete chromosomes – with conceptual models for the elaboration of chromatin fibre structure supported by *in vitro* studies (Fig. 1). Chromatin experiences a hierarchy of packaging but the models become increasingly speculative as the volume of observation increases. Chromatin carries negative charges due to incomplete neutralisation of the DNA polymer's phosphate backbone by basic core histones. The result is that chromatin structure is subject to electrostatic repulsion between its neighbouring sections. Chromatin also responds to changes in the electrostatic microenvironment which interacts both with negatively charged DNA and the positively charged histones. As a result chromatin structure can be manipulated *in vitro* by simply changing the electrostatic environment, frequently by supplying divalent cations. In live cells these fundamental properties contribute to a state of fluidity – perceived as a ‘liquid-like behaviour’ of the 10-nm chromatin fibre (21). The 30-nm chromatin fibre is often regarded as the secondary structure of chromatin directed by nucleosomes, nucleosome-protein complexes and regulatory factors (22). This key structure remains controversial both in its form and the extent to which it is adopted in different cells types (23,24). However, even at these primary and secondary levels, it is recognised that the

chromatin structural environment does not remain static. In live cells chromatin transitions can occur on timescales which range from milliseconds to minutes or even hours (25).

For a DNA probe to work it must reach its target. Inadequate target exposure can also be a factor in the pharmacodynamic failure of a drug. Predicting access to intracellular targets can involve a label-free (26) or fluorescent drug-based modelling approaches (27). However, such methods are yet to consider the impact of the chromatin 'labyrinth' (26). Chromatin structures present an 'obstacle network' for diffusing proteins, effective over a distance of 1–2 μm , providing a temporal restraint on interactions with DNA (20). It remains unclear whether 'obstructed transport' through chromatin networks (28) can predict probe/drug access to DNA targets. The caveat is that a probe may be limited by the chromatin states it can report – a source of unsuspected bias. The stress responses of chromatin control chromatin accessibility to facilitate genome stability (29). For example, the 'relaxation' of chromatin at regions of damaged DNA signals damage location and promotes the assembly of repair complexes (30). Nucleosomal structure itself can be considered both a 'central signalling hub' and a 'landing platform' in the repair process (31). A range of fluorescence imaging methods can now provide descriptions of DNA repair in single cells [review: (32)]. Fluorescent probes for marking sites of DNA damage can provide insights into defects in DNA repair. Such approaches include detection of base excision repair intermediates (apurinic/apyrimidinic sites) in DNA (33) and dual-incision steps of UV-damaged cellular nucleotides (34) in combination with flow cytometry.

Chromatin dynamics

Chromatin remodelling encompasses multiple activities including: DNA replication and repair, transcriptional control, epigenetic regulation, programmed disassembly during apoptosis, chromosome packaging and segregation. These events are clearly relevant to critical cellular transitions in development, neoplastic progression and pluripotency (20,35-37). A current view is that regulation of the chromatin nano-environment, over ranges that exhibit chromatin packing-density heterogeneity, can allow for a predictable modulation of global patterns in gene expression (38). A 'rational' modulation of chromatin density fluctuations can lead to a decrease in global transcriptional activity. One can view this as 'macrogenomic engineering' within the nucleus for directing whole-scale transcription levels (38).

ATP-dependent nucleosome-remodelling complexes direct histone behaviour through an ATPase-translocase 'motor' function that mobilises DNA within the nucleosome (39). ATP-dependent enzymes that remodel chromatin are therefore important controllers of structure (36,40,41). Key functional components of chromatin, along with histones, condensins, cohesins and regulatory proteins (42-44), are the distinct class of topology correcting enzymes – the DNA topoisomerases. Chromatin is a store of torsional energy which results in the release of negative superhelicity upon decompaction (45). Conversely, dynamic changes in DNA supercoiling will dictate packaging and transcription (46). Nuclear problems can arise when the replication of chromatin loops generates interlinked DNA products (catenanes) or when DNA function requires the resolution of torsional stress. The cell's enzymatic solution is via the DNA topoisomerases. These enzymes provide a co-ordinated process of

strand passing within a DNA-enzyme complex (type IA and type IB enzymes). They can also allow the movement of an actively-cleaved strand around an intact strand prior to re-ligation (type IB enzymes). Type IIA enzymes are 'full decatenases' (40), passing one duplex through a double-strand break generated by the enzyme in another duplex. On the other hand, type IA enzymes strand pass single-stranded DNA segments by the adjacent duplex and thereby locally changing the linking number (40). Type IIA DNA topoisomerases are vital for progression through the cell cycle (47). In terms of probe manipulation of superhelicity, intercalation can generate changes in local supercoil relaxation states with extension of the duplex. A cell permeant biotinylated 4,5,8-trimethylpsoralen probe, that preferentially intercalates with DNA enriched in negative supercoils, has been used to monitor changes in DNA supercoiling in vivo (45). RNA polymerase and topoisomerase activities remodel DNA supercoiling, creating supercoiling domains that affect the folding of large-scale chromatin structures (45).

The DNA topoisomerases present specific and demonstrable targets for several classes of both anticancer and antibacterial drugs (41). A flow cytometry-based method has been described for the high-throughput analysis of drug-stabilized topoisomerase II cleavage complexes in human cells (48). In mammalian cells the DNA damage signalling responses to DNA topoisomerase inhibition can also be tracked by flow cytometry to reveal the restraints on DNA replication and cell cycle progression (49-51). The human type IIA enzyme is a target for catalytic inhibitors such as the bis-dioxopiperazine ICRF-193. ICRF-193 induces late cell cycle checkpoint stalling, decatenation inhibition, mitotic anomalies or even bypass of mitosis to polyploid states in permissive cells (52). Recent structural analyses indicate how type IIA enzymes embrace the helix DNA and how the enzyme-DNA interactions inform drug behaviour (53). The human type IIA topoisomerase proteins, topoisomerase II α (Top2alpha) and topoisomerase II β (Top2beta), are the targets for several anticancer agents including etoposide, the DNA intercalating anthracyclines (doxorubicin, daunorubicin) and the anthraquinone mitoxantrone (54). The cellular roles of topoisomerase II β (55) and the consequences of inhibition, given its expression in terminal differentiation, are less understood compared with the cell cycle regulated topoisomerase II α . Bacterial type II topoisomerases (gyrase and topoisomerase IV) are the targets of quinolones and aminocoumarin antibiotics (41).

The eukaryotic type IB topoisomerases (Top1) are classically targeted by camptothecin and related derivatives such as topotecan or irinotecan. Genome-wide high-resolution mapping has revealed the targeting of transcriptionally active genomic regions by the Top1 inhibitor topotecan and the Top2 inhibitor etoposide. On the hand, daunorubicin induces DNA breaks and evicts histones from active chromatin with a 'quenching' of local DNA damage responses (56). Fluorescence lifetime imaging microscopy (FLIM) has been used to map the nuclear docking of topotecan at a subset of DNA sites in nuclear structures of live breast tumour cells in which the DNA binding probe DRAQ5 has been used to uncover sites of drug interaction (57). The anticancer anthracyclines daunorubicin (daunomycin), doxorubicin (adriamycin) and epirubicin (4'-epi-doxorubicin, an active isomer of doxorubicin), belong to a class recognized as potent Top2 'poisons'. Their ability to generate protein-associated dsDNA breaks can be detected by cytometric analysis (40). Early studies showed the restricted binding of the anthracycline doxorubicin to DNA within chromatin compared to calf thymus free DNA and the ability of related drugs to induce compaction of isolated chromatin (58,59). Further evidence indicates that anthracycline antibiotic exposure can lead to chromatin unfolding and aggregation (60), DNA torsional changes (61) and histone eviction from open chromatin (62). Such drugs are also self-reporting probes

for cellular and nuclear micro-pharmacokinetics enabled by their intrinsic fluorescence tracked in real-time by flow cytometry (63,64).

Resolving chromatin organisation:

Super Resolution Optical Microscopy

New developments in fluorescent sensors based on small-molecule dyes or fluorescent proteins (13) are in parallel with expanding options for advanced microscopy methods for visualizing chromatin structure (4). Fluorescent sensors for monitoring proteins, DNA, RNA, small molecules and ions (e.g. Zn^{2+}) can all exploit super-resolution microscopy (13). Some of these approaches are noted briefly here. Super-resolution fluorescence microscopy encompasses multiple techniques (65) that are applicable to probing chromatin structure (4,66-70). Super-resolution microscopy effectively breaches the diffraction limit of optical microscopy and efforts continue to accrue techniques reaching signal resolution at length scales of sub-20 nm. Typical approaches employ the principles of patterned illumination light, such as Saturated Structured Illumination Microscopy (SIM) and Stimulated Emission Depletion (STED). Alternatively, some methods such as Stochastic Optical Reconstruction Microscopy (STORM), Photoactivation Localization Microscopy (PALM), and fluorescence-based fPALM allow for single molecule detection and localization applicable to the imaging of chromatin organisation (4). Approaches include the use of a fluorescent label to image DNA and chromatin *in situ* at the single-molecule level (71-73). A recent application of the DNA dye Vybrant®DyeCycle Violet with single molecule localization microscopy (SMLM) has generated images of DNA in nuclei of fixed mammalian cells (74). It is estimated that using fixed whole cells and standard DNA dyes, a structural resolution of chromatin is attainable of the order of 50-100 nm using SMLM (72). The use of Spectral Precision Distance/Position Determination Microscopy (SPDM) has the potential to reveal nuclear nanostructures down to few tens of nanometre resolution (75). Several intercalating and minor-groove binding DNA dyes can be used to register (optically isolate) a few DNA-binding dye signals at a time using a variation of Binding-Activated Localization Microscopy (BALM) (71). We should also remember that unmodified nucleic acids can show stochastic fluorescence switching at physiological concentrations under visible light illumination. This presents an opportunity for label-free super-resolution imaging of DNA directly (76). However, at this stage super-resolution approaches cannot address the problem of how to visualise and reconstruct chromatin ultrastructure through large 3D volumes of intact cells – a problem familiar in cytometry.

ChromEMT

The practical limits on imaging resolution restrict the ability to visualise chromatin organisation *in situ* for informative 3D volumes. A recent report has broken through this analysis barrier for intact cells using a new method. ChromEMT enables DNA and chromatin ultrastructure to be visualized and reconstructed unambiguously through large 3D volumes (77). The ChromEMT method combines electron microscopy tomography (EMT) with a labelling method that selectively enhances the contrast for DNA structures. The ChromEMT technique exploits unique properties of the fluorescent anthraquinone DNA dye DRAQ5, which upon photon-activation can catalyse the deposition of diaminobenzidine (DAB) polymers on the chromatin surface, enabling structures to be subsequently

visualized with OsO_4 in EM [Figure 2; (77)]. DAB photo-oxidation has been used in a range of studies that correlate light and electron microscopy, for nanoparticle location and the residence of low levels of photosensitizing molecules (78). Advances in multi-tilt EMT have allowed researchers to reveal the chromatin ultrastructure and 3D packing of DNA in both human interphase cells and mitotic chromosomes. Critically, it appears that there is a disordered nature of the chromatin chains revealed by ChromEMT. These chains are flexible, bending and folding into different packing densities. Dynamic changes in packing density provide opportunities to fine tune accessibility to DNA sequences, nucleosome variations and chromatin modifications. These variations in packing density will be important at both local and global levels within the intact nucleus. This opens a new level of organisation or indeed dis-organisation for exerting control over function. The anthraquinone dye used in ChromEMT recalls a lineage of molecules that link probe and drug properties employed in nuclear cytometry.

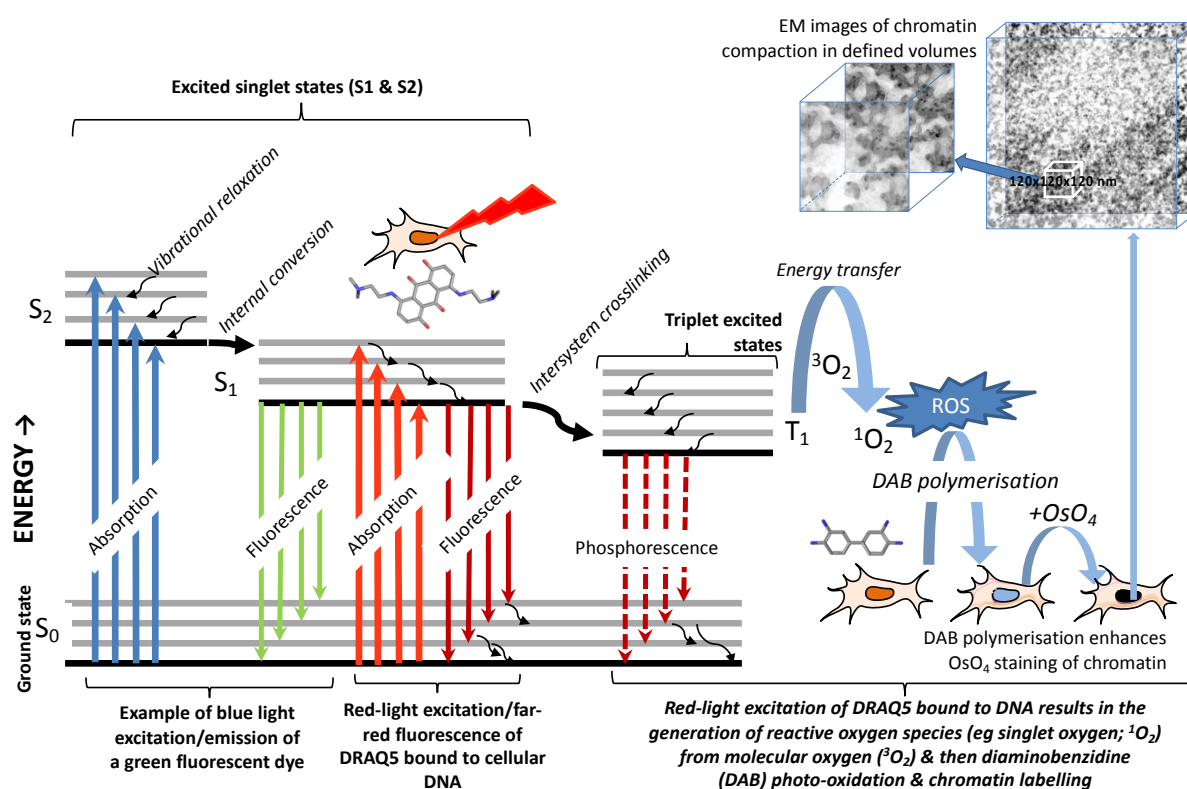


Figure 2. ChromEMT: Jablonski energy diagram of DRAQ5 excitation, fluorescence and the formation of a triplet excited state generating reactive oxygen species (ROS) that enable subsequent chromatin

visualisation at low scalar distances. Diagrammatic sequence shows the photo-oxidative catalysis of the deposition of osmiophilic DAB polymers on DNA in chromatin in situ (77).

Nuclear cytometry: DNA reporting

The measurement of cellular DNA content, a common laboratory procedure (12,79), has been dependent upon the stoichiometric reporting capacity of fluorescent nucleic acid-affinic dyes.

In terms of nuclear cytometry, several classes of 'vital' DNA fluorescence probes, in addition to the bis-benzimidazoles Hoechst™ dyes offer the ability to explore chromatin dynamics in live cells. This expanding palette of probes includes: Syto61™, DRAQ5™ and Vybrant® DyeCycle™. The interactions of a range of fluorescent dyes such as quinacrine, Hoechst 33258 (80), daunomycin, chromomycin A3 and 7-aminoactinomycin D with DNA offer multiple probe-based approaches for exploring chromatin structure (5). A recent addition to the suite of small-molecule fluorophores is the near-infrared (IR) silicon-rhodamine dyes with spectral properties that aid in vivo imaging (81). Spectral analysis can reveal modes of binding, sequence selectivity, probe interactions, consequences of fixation and selectivity of nuclease digestion. At a fundamental level, probe performance can be expected to obey the law of mass action in relation to unbound fluorochrome concentration (12). In studies on anticancer drugs there is always the possibility of interaction between the drug and the fluorochrome used to simultaneously probe DNA content. Since some of the DNA-binding drugs are fluorescent, their emission can directly overlap with that of the probe, through Förster resonance energy transfer, and affect the efficiency of probe detection (82).

With all probes there are caveats. Prolonged exposure of live cells to the nominally non-permeable dye propidium iodide (PI) reveals a background granular distribution of the probe in the cytoplasm, consistent with accumulation in endosomes, and also dye binding to nucleolar RNA in live cells (83). DAPI (4',6-Diamidino-2- phenylindole dihydrochloride) is usually referred to as a semi membrane-permeant dye because of its reduced penetration through viable cell membranes but it is concentration sensitive with respect to toxicity especially at levels for attempts at DNA content reporting (84). A non-permeable very low toxicity dye, such as DRAQ7, offers the opportunity to monitor subpopulations of cells that lost cellular barriers to chromatin access but without perturbing the viable cell fraction (85). This approach is particularly useful when monitoring transitions in cell behaviour (86). In the case of the of vital cell dyes, problems of cell proliferation inhibition (14) and phototoxicity (87) can arise, but these effects will be time, dose and system dependent. The anthraquinone DRAQ5 when used at levels that reveal efficient DNA content reporting in live cells can interfere with the binding of H2B core histones to DNA, not observed after binding to DNA of a minor groove binder Syto17 (88,89). Hoechst 33342, DRAQ5, and DyeCycle Violet induce various degrees of DNA damage responses and cell cycle changes, which should be a matter of concern when using these dyes as supravital DNA probes inappropriately (90). Photo-toxicity of dyes is an issue. This is particularly the case a shorter wavelengths as observed with UV-excited Hoechst 33342 in time-lapse fluorescence microscopy (87). However, this known 'adverse' effect of UVA irradiation on dye-treated cells can be used to investigate the kinetics of dye residence at critical chromatin sites capable of generating photo-induced DNA-protein crosslinks (91). The potential for photosensitisation is

appreciated in the context of photothermal therapy (PTT) and photodynamic therapy (PDT). Here there have been recent advances in the synthesis and application of NIR-absorbing organic nanoparticles as phototherapeutic ‘nanoagents’ (92).

Small DNA-affinic molecules can be used to reveal not only DNA content but also accessibility within higher orders of chromatin structure. This opportunity was recognised in earlier cytometry studies (93) by exploiting the metachromatic properties of acridine orange (AO) (94,95). Many of our current methodological approaches and signal interpretations were developed using this cytometric probe. Differences in chromatin structure can be revealed by the metachromatic effects detecting DNA ‘melting’ – the differential susceptibility of DNA *in situ* to undergo denaturation upon exposure to heat or acid. Differential stainability of dsDNA (green fluorescence) *versus* ssDNA (red fluorescence) with AO made it possible to discriminate between G_0 , G_1 , S, G_2 and M cells (94,95) (Fig. 3). Multiple cytometry techniques have been applied to cell cycle profiling, including exploitation of chromatin-protein bindings events, chromatin modification and the nuclear translocation of cyclins. DNA content and chromatin-bound proteins to reveal sub-phases in G_1 (96). Mass cytometry using 5-iodo-2-deoxyuridine (IdU) can co-mark cells in S phase using cyclin antibodies and the phosphorylation patterns a specific histone H3 (97). Live cell tracking of a cyclin B1-GFP sensor can detect cell-cycle phase routes to mitotic traverse, arrest or endoreduplication confirmed by flow cytometric mapping using DRAQ5 (98).

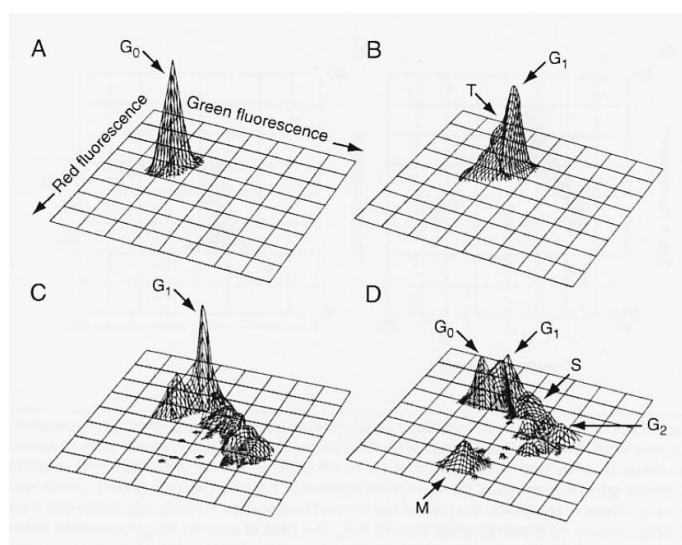


Fig. 3. Cytometric analysis showing differences in chromatin structure of lymphocytes in different phases of the cell cycle. Sub-sets revealed by changes in susceptibility of DNA to denaturation induced by acid followed by differential staining of dsDNA versus ssDNA with metachromatic fluorochrome acridine orange (AO). (A) Unstimulated cells, (B) cells stimulated with phytohemagglutinin (PHA) for 18 h, (C) cells stimulated for 3 days, (D) cells stimulated for 3 days; vinblastine included in the cultures for the final 6 h to arrest cells in mitosis. Evident is the transition (T) cells from G_0 to G_1 after 18 h, associated with an increase in green fluorescence and a decrease in red. Subpopulations of cells in G_0 , G_1 , S, G_2 and M can be distinguished based on changes in green and red fluorescence (94,95).

Fluorescent dye-chromatin interactions borrow from the experience with chromosome banding. These can reveal the spectacular capacity of cells to show shifts in chromosome organisation at its highest levels (99,100). At a highly practical level, metachromatic staining by AO reveals any defective packaging of DNA in chromatin of infertile sperm cells (101). Fig. 4 shows the classic flow cytometry methodological study of human fertile versus infertile sperm cells (102). Defective packaging of DNA correlates with DNA fragmentation, not unlike that seen in apoptotic cells (103,104). This methodology was adopted in clinical practice for detecting fertility status of human males and in animal husbandry (105,106).

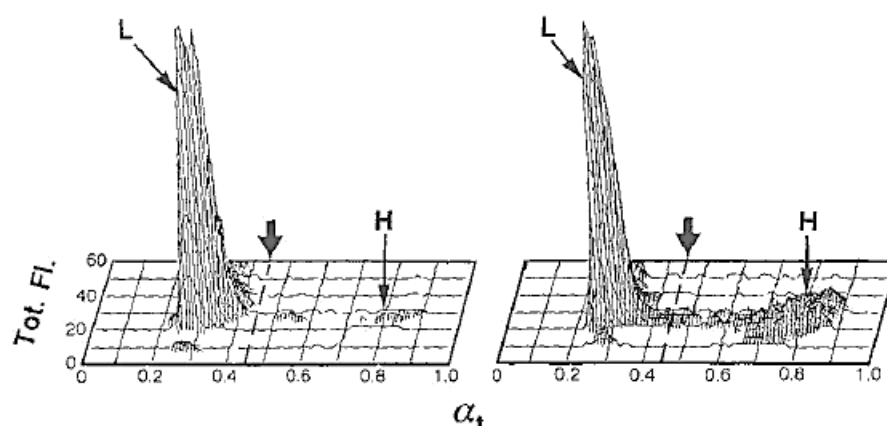


Figure 4. Susceptibility of DNA to denaturation as detected by staining with AO reveals the presence of human sperm cells with defective chromatin structure (H) correlated with infertility. *Bivariate frequency distribution histograms representing intensity of total fluorescence (Tot. Fl.; red+ green) versus α_t (ratio of red to total fluorescence intensity) of two samples of sperm cells, one characterized by a small fraction of cells with high sensitivity of DNA in situ to denaturation (left) and the other with a higher proportion of such cells (right). The borderline discriminating between the cells characterized by low (L) and high (H) sensitivity to denaturation (α_t index) is marked by thick arrows. The frequency of H cells in infertile subjects was shown to be correlated with frequency of cells with fragmented DNA detected by the TUNEL assay (103).*

In the native nucleus, the extent and modes of binding of DNA interacting agents are informed not only by agent properties and chromatin access but also by cellular routes for handling small molecule probes. For example, contrast to fixed cells, live cells exposed to AO at low concentrations (<5 μ M) selectively accumulate the probe in acidic vesicles, including lysosomes where it luminesces red, and is not a useful chromatin probe (107,108). The situation is complicated further by dynamic chromatin structures responding to the presence of a probe/drug itself and linked downstream stress responses. Not surprisingly there is significant interest, in both nuclear cytometry and anticancer targeting strategies, to gain an understanding of critical chromatin structures and their perturbation.

Nuclear cytometry: alternatives

Not all methods depend upon the intrinsic or enhanced fluorescence of a probe or indeed that of a nuclear-locating drug. Mass cytometry has exploited metal-based unique signals for DNA-affinic molecules for: the study of cellular uptake and the linked anticancer effects of platinum-containing drugs (109), the use of cisplatin-antibody-conjugates for immunophenotyping (110) and the incorporation of a platinum-based covalent reagent to act as a discriminator in cell viability measurements (111). Alternative detection modalities can assess the subcellular disposition of reporter probes. Raman spectroscopy as applied to microscopy has been used to measure the chemical signature of a sample or identify the presence and quantity of a molecular species (112) (Figure 5). The characteristics and behaviour of a probe can in turn be used to extract biological information via the state of the probe at specific locations. The two typical methods of collecting the Raman spectral data to generate images are Raman mapping and Raman imaging. Raman mapping collects a spectral hypercube (a Raman spectrum from each position on the sample in a single file), rather than a simple intensity image. The hypercube is analysed to produce Raman images. There are several Raman mapping methods, including point-by-point mapping and line focus mapping. Here, there is a balance between under-sampling and acquisition time for sample regions of interest. Spatial resolution is determined by a combination of the laser spot size and the spacing between acquisition points on the sample (e.g. sample stage step sizes down to 100 nm). On the other hand, Raman imaging allows for rapid acquisition, by collecting spectral intensity values simultaneously from an entire region of interest, especially if high laser power is available. However this approach yields limited information with an ultimate resolution to a little under a micrometre.

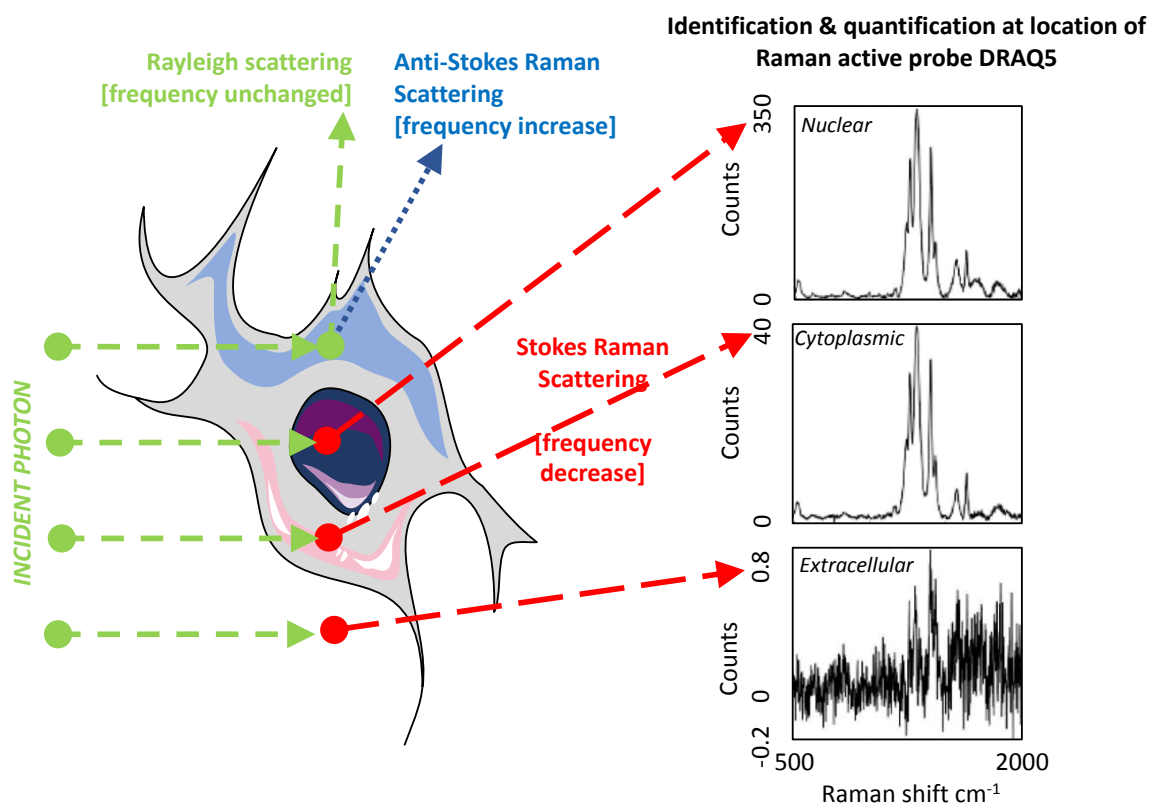


Figure 5: Diagrammatic representation of some of the light scattering modes of interest and the differential detection of a Raman signature for a cell permeant DNA binding probe. *The more familiar Rayleigh scattering can be described as ‘elastic’ scattering since the photon energies of the scattered photons are not changed. When a Raman active probe is irradiated with photons of a selected frequency, that avoids peak fluorescence excitation, a minority of the incident photons interact with a vibrational mode of the irradiated probe and are ‘inelastically’ scattered. The inelastically scattered photons are shifted in frequency. This shift can be to a higher frequency (anti-Stokes) or to a lower frequency (Stokes). The frequency versus intensity Raman spectrum provides a unique detection signal for the probe at a selected location. (Acknowledgement: exemplar data for DRAQ5 provided courtesy of L Jamieson, D Graham & K Faulds, Centre for Molecular Nanometrology, Department of Pure and Applied Chemistry, University of Strathclyde, UK).*

Many materials have characteristic Raman spectra, with a growing number of applications within biology. The approach can provide chemical and compositional information and does not typically suffer from interference from water molecules. Further, cellular components, including DNA, have distinct intrinsic Raman scattering spectra (113). Chromatin density variation among the individual sub-phases of mitosis affect Raman and infrared micro-spectroscopic intensities (114). Label-free DNA imaging in vivo has been demonstrated using stimulated Raman scattering microscopy (115,116). Hyperspectral Coherent anti-Stokes Raman scattering (CARS) microscopy (117) can be used to provide label-free quantitative volumetric imaging of cell composition defined in terms of water, protein, chromatin and lipids (Fig. 6).

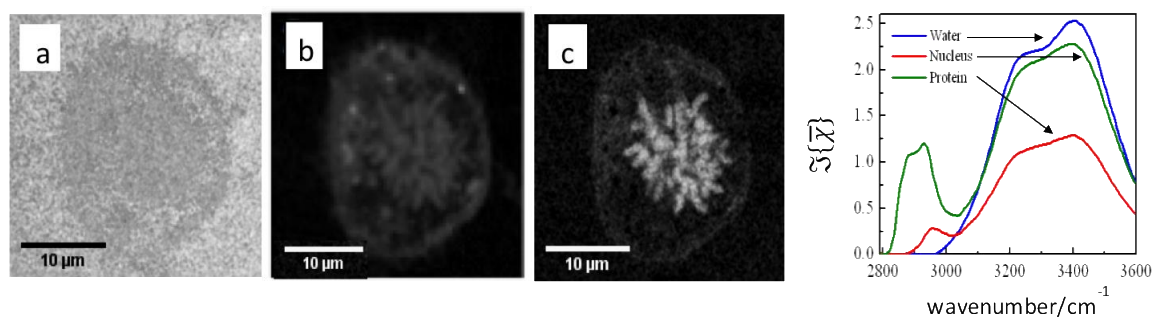


Figure 6 Hyperspectral CARS of a mitotic cell - detection of key cellular components and their spectra in a human osteosarcoma cell. *Cells were imaged in 3D in the CH stretching vibrational range ($\omega=2400-3800\text{ cm}^{-1}$) using a 60X 1.27NA water objective and 1.4NA oil condenser. The point spread function (PSF) informs the imaged volume for chemical components [volume dimensions of approximately $0.3\text{ }\mu\text{m}$ lateral and $0.9\text{ }\mu\text{m}$ axial full width at half maximum (FWHM)]. Note that the imaged volume contains about 95% water. Y axis shows hyperspectral averaged $\mathcal{S}(\bar{\chi})$ data (118). To analyze the data, a three step method was applied which includes singular value decomposition (SVD), phase corrected Kramer's Kronig (PCKK)(118) and factorization into susceptibilities and concentrations of chemical components (FSC3) [(a: blue = water; b: green = protein; c: red = DNA)]. (Unpublished: exemplar data by A Karuna, F Masia, P Borri, R Errington, and W Langbein at the Schools of Physics, Biosciences and Medicine, Cardiff University, UK).*

Mass Spectrometry Imaging (MSI) can qualitatively describe drug distribution in 2D tissue sections while 3D MSI can reveal the heterogeneity in tumours (119). MALDI imaging mass spectrometry has been applied to the analysis of the spatial distribution of histone modifications in tissues (120), with recent studies achieving high lateral resolution of the order of 5 micrometre approaching a cell-to-cell methodology. Partial-wave spectroscopic (PWS) microscopy is a label-free quantitative imaging technique (resolution range of 20 and 200 nm), capable of tracking changes in chromatin structure after DNA damage in live cells (121). This approach reveals that UV-excited Hoechst 33342 can cause damage to chromatin within seconds. Over a time-frame of minutes, the dye itself can cause a global alteration in chromatin nano-architecture independent of its excitation (121). PWS microscopy reveals the not unexpected chromatin disrupting effects of fixation (122). This disruption highlights the relevance of live cell imaging techniques, or the advantage of cryo-fixation, when exploring native chromatin organisation (122). The ability to combine PWS microscopy with fluorescence confocal microscopy for the co-localization of cellular nanostructures is a welcome route for functional annotation (123). Alternative modes of light interaction with DNA dyes can be exploited in nuclear cytometry. For example, the unique light absorption properties and high DNA affinity DRAQ5 (124) coupled with low fluorescence quantum yield (125), have been exploited in hybrid ultra-high frequency acoustic/photoacoustic microscopy. The generation of photoacoustic signals from a cell's nuclei reveals gross conformation and nuclear dimensions (126).

Apoptosis, autophagy & NETs

Chromatin disassembly is a feature of the various cell death processes and will only be discussed here briefly. Multiple cytometric methods can track the irreversible apoptotic process of chromatin disassembly (127,128) and real time progression to the '*fait accompli*' of plasma membrane disruption (85). In the case of apoptosis, nuclear DNA undergoes extensive fragmentation and release from the cell within apoptotic bodies (42). RNA and DNA are segregated and packed into separate apoptotic bodies (129) detectable in peripheral blood (130). Specialization of phagosomes of macrophages facilitates heterophagic degradation of nucleic acids during apoptosis (129). An exciting and emerging area is the balance between autophagy, providing an environment for cell survival, versus the enactment of cell death processes via apoptosis. The cell survival and housekeeping process of autophagy involves the breaking down and reusing of cytoplasm components. Fluorescence microscopy and flow cytometry is commonly used to study autophagy of discrete structures such as mitochondria (131) and lysosomes (107). Flow cytometric methods are also available to detect the linked changes in organelle mass using MitoTracker Green (MTG) and Endoplasmic Reticulum Tracker Green (ERTG) (132). Evidence is mounting that there is cross-talk between the dysfunction of apoptotic and autophagic pathways in disease states including neurodegeneration (133) and cardiac pathology (134). Participants in this cross-talk are modifications to histones, providing critical structural codes (135).

Chromatin 'function' or rather 'value' can extend beyond the cell's boundary (136) presenting a distinct focus area for cytometry. The cell death process termed NETosis, creates homogenised

chromatin together with granule proteins that undergo release from actively disintegrating neutrophil granulocytes. A variety of triggers promote NET formation. These chromatin structures form a tethered extracellular mesh (Neutrophil Extracellular Traps; NETs; (137)). NETs enmesh and degrade virulence factors and kill bacteria. The DNA backbone of NETs is vulnerable to extracellular DNase digestion. Although NETosis is distinct from apoptosis and necrosis, there is conflicting evidence of its dependence on autophagy for extracellular DNA trap formation (138,139). Further there is a distinction between the formation of NETs from mitochondrial or nuclear DNA (140). Nuclear chromatin-originating DNA masses are less structured (the DNA mass being some 3-5-fold greater in volume than condensed chromatin) and less beneficial for antimicrobial trapping (141). The more structured mitochondrial originating NETs are built around the tight packaging of mtDNA as nucleoids and their organization into higher-ordered assemblies (142).

Developing cytometric methods that distinguish different NET origins and structures have applications in measuring inflammatory vascular injury and tissue damage (143) and in a variety of disease processes including autoimmunity, thrombosis, cancer and antiviral responses (144). NET formation has been examined using correlative microscopy - combining TEM, SEM, immunofluorescence and live cell imaging techniques (145). Such imaging approaches can be supported by automated image quantification software (146). A range of probe-based methods are also available for quantifying NETosis (145,147). They include flow cytometry and staining with the plasma membrane-impermeable DNA-binding dye SYTOX Green and its correlation with image-based detection (148). Co-staining for DNA (DAPI) and myeloperoxidase positivity has also been used (149). DRAQ5 and SYTOX Green staining patterns can enable NET detection by both flow cytometry (150) and imaging (151). DRAQ5 and human neutrophil elastase immunostaining and microscopy have been used to profile NETs capturing *Candida albicans* yeast cells (152). An interesting recent approach uses the ImageStream® platform (Millipore Sigma, Darmstadt, Germany) detecting the morphology of DRAQ5-stained NET DNA trails tethered to the remaining cell structure (153).

One man's probe is another man's poison

In vivo probes and drugs have to deal with adverse extracellular microenvironments (154) and a metabolic environment frequently determined by gene expression patterns (e.g. p450 family; (155)). These states can enhance or even frustrate delivery to targets (154). For example cytometry has revealed the DNA targeting potential of fluorescent anthraquinone-based prodrugs (156,157) in their response to their metabolic activation in hypoxic microenvironments (158). Flow- and image-assisted cytometry can profile individual molecular events in DNA damage responses (159) linked to effective targeting of a probe (160) or cross-resistance to a drug (161). The ability of drug molecules to quench Hoechst 33342-DNA fluorescence signatures can be used to track the binding of molecules with low fluorescence [e.g. the anti-leukemic drug 4'-(9-acridinylamino) methane sulfon-m-anisidide; m-AMSA; (162)] or spectrally distinct fluorescence properties (125,163). DNA targeting agents face cellular membrane barriers (112,164), active efflux (161) and sequestration at cytoplasmic sites (156). The nucleic acid target is clearly in competition with different kinds of molecules. Even the packaging of the genome by histone proteins into nucleosomes can alter how different DNA sites interact preferentially with an agent. A DNA affinic drug such as mitoxantrone (MTX) can significantly impact

upon chromatin protein residence and function (51,165,166), DNA topoisomerase function (167). The pharmacodynamic effects of MTX appear to be dependent upon persistence at the chromatin target (54) an indicator that probe residence time at target is critical. Probe efflux provides information on cell heterogeneity that can correlate with drug response heterogeneity. The detection of 'side-populations' characterizing stem cells (168) is based on the extent of the binding-dependent shift in the Hoechst 33342-DNA emission spectrum (169,170). Changes in Hoechst 33342 (171,172) and Vybrant® DyeCycle™ Violet (173) cellular fluorescence effectively track dye efflux capacity. The efflux signature of DNA interactive agents and drugs can be explored using a compartmental modelling approach, providing a mathematical description of the activity of the anti-cancer agent. Such models can take into account intracellular modification and delivery to a nuclear DNA target (27). This can also be extended to model the subsequent perturbation of the cell cycle (174). Smart DNA-targeted reporters will enable mathematical constructs of single cells that link Micro-Pharmacokinetics and cellular Pharmacodynamics with specific Cellular Descriptors (μ PK-PD-CD). Descriptors, such as aldehyde dehydrogenase enzyme expression (175), bring a finer cytometric dimension to early drug development (176).

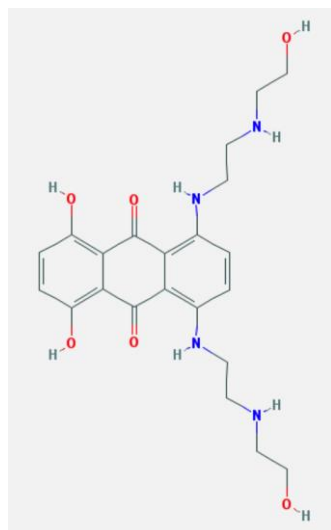


Figure 7: Chemical structure of Mitoxantrone (MTX) - an anthracenedione antibiotic with antineoplastic activity. Chemical structure information and properties are obtainable from the PubChem Substance and Compound databases (177).

The problem of understanding the biological impact of a DNA targeting molecule and probe properties in the context of chromatin structure has exemplified here by the anthracenediones. Mitoxantrone (MTX; Novantrone®), (1,4-dihydroxy-5,8-bis[[2-[(2-hydroxyethyl)amino]ethyl]amino]-9,10-anthracenedione) is an anthracenedione - structurally related to the classical anthracyclines. MTX has also provided an impetus for the generation of derivatives including prodrug forms (178-181) for a more selective targeting of tumour cell populations (182). Its behaviour in the chromatin environment (166) is an exemplar of multi-level action (40). A principal mechanism of action of MTX is the persistent inhibition of DNA topoisomerase complexes (54). However, MTX also has a striking ability to condense nucleic acids by both trapping and excluding chromatin proteins (166,183). The MTX chromophore ($\text{Ex}\lambda_{\text{max}}$ 610 and 660 nm; $\text{Em}\lambda_{\text{max}}$ 685 nm ; (184)) permits fluorescence microscopy and flow cytometry to determine uptake and nuclear distribution revealing drug resistance (185) and the behaviour of alkylamino-anthraquinones derivatives and their N-oxides (156). The structurally related far-red fluorescent DNA dyes and the nuclear counterstains DRAQ5™ (124,186-188), DRAQ7™

(85,128,189-191) and the spectrally shifted CyTRAK Orange™ (192) have applications in nuclear cytometry (193). The spectrally-compatible combination of the nuclear stain DRAQ5 and the anionic counterstain eosin also provides a dual-component fluorescent staining protocol. This is analogous to haematoxylin & eosin and intended for use on fresh, non-sectioned tissues (186) in clinical settings – an innovation loop in nuclear cytometry that now spans centuries (194).

Conclusion

In terms of nuclear cytometry there is a widening of the opportunities to deploy smart molecular DNA probes, not restricted by their fluorescence profiles. Novel probes offer distinct and often unique properties. Molecular probe design is clearly informed by drug development highlighting a constant caveat for the use of vital probes, in which their biological effects can be a known unknown. The ambition here is to reveal fundamental aspects of nuclear function and chromatin form. New opportunities arise from understanding the photophysical and photochemical properties of probes in conjunction with the targeting of discrete biological structures while also exploiting new detection modalities. Downstream impact lies in the promise of methodologies that can inform chromatin structures and organisational levels that are targets for anticancer drugs or indeed reflect disease progression. Further, using these new approaches to nuclear cytometry, to describe the chromatin changes that occur both globally and locally during key transitions such as a somatic to pluripotent states (195,196), will reveal the extent to which such changes have regulatory roles in both disease and health.

Declaration & Acknowledgements

Authors PJS and RJE declare that they are non-executive directors of Biostatus Ltd, the commercial supplier of DRAQ5, DRAQ7 and CyTRAK Orange. ZD has no conflicts to declare. The authors note: Vybrant® DyeCycle™ Ruby stain Syto61™ are trademarks of Thermo Fisher Scientific USA (Molecular Probes Inc.); MitoTracker™ and ER-Tracker™ are registered trademarks of Molecular Probes, Inc.; DRAQ5™, DRAQ7™ and CyTRAK™ are trademarks of Biostatus Ltd; Hoechst™ is a trademark of Sanofi

USA; ®Adriamycin is a registered trademark of Pharmacia & Upjohn S.P.A.; Novantrone is a trademark American Cyanamid Company. Chemical structures are obtainable from the PubChem Substance and Compound databases (177). ZD is supported by The Robert A. Welke Cancer Research Foundation.

References

1. Flors C. Super-resolution fluorescence imaging of directly labelled DNA: from microscopy standards to living cells. *J Microsc* 2013;251:1-4.
2. Gabbay EJ, Wilson WD. Intercalating agents as probes of chromatin structure. *Methods Cell Biol* 1978;18:351-84.
3. Horobin RW, Stockert JC, Rashid-Doubell F. Uptake and localisation of small-molecule fluorescent probes in living cells: a critical appraisal of QSAR models and a case study concerning probes for DNA and RNA. *Histochem Cell Biol* 2013;139:623-37.
4. Lakadamyali M, Cosma MP. Advanced microscopy methods for visualizing chromatin structure. *FEBS Lett* 2015;589:3023-30.
5. Latt SA. Fluorescent probes of chromosome structure and replication. *Can J Genet Cytol* 1977;19:603-23.
6. Levi V, Gratton E. Chromatin dynamics during interphase explored by single-particle tracking. *Chromosome Res* 2008;16:439-49.
7. Lurquin PF. The use of intercalating dye molecules in the study of chromatin structure. *Chem Biol Interact* 1974;8:303-12.
8. Schweizer D. Counterstain-enhanced chromosome banding. *Hum Genet* 1981;57:1-14.
9. Forment JV, Jackson SP. A flow cytometry-based method to simplify the analysis and quantification of protein association to chromatin in mammalian cells. *Nat Protoc* 2015;10:1297-307.
10. Galbraith DW, Sliwinska E, Samadder P. Nuclear Cytometry: Analysis of the Patterns of DNA Synthesis and Transcription Using Flow Cytometry, Confocal Microscopy, and RNA Sequencing. *Methods Mol Biol* 2018;1678:371-392.
11. Smith PJ. Cytometric routes to single cell transcriptomics. *Cytometry A* 2016;89:424-6.
12. Darzynkiewicz Z. Critical aspects in analysis of cellular DNA content. *Curr Protoc Cytom* 2010;Chapter 7:Unit7.2.
13. Specht EA, Braselmann E, Palmer AE. A Critical and Comparative Review of Fluorescent Tools for Live-Cell Imaging. *Annu Rev Physiol* 2017;79:93-117.

14. Wink M. *An Introduction to Molecular Biotechnology: Fundamentals, Methods and Applications*: John Wiley & Sons; 2013.
15. Almassalha LM, Tiwari A, Ruhoff PT, Stypula-Cyrus Y, Cherkezyan L, Matsuda H, Dela Cruz MA, Chandler JE, White C, Maneval C and others. The Global Relationship between Chromatin Physical Topology, Fractal Structure, and Gene Expression. *Sci Rep* 2017;7:41061.
16. Gilbert N, Boyle S, Fiegler H, Woodfine K, Carter NP, Bickmore WA. Chromatin architecture of the human genome: gene-rich domains are enriched in open chromatin fibers. *Cell* 2004;118:555-66.
17. Nozawa RS, Boteva L, Soares DC, Naughton C, Dun AR, Buckle A, Ramsahoye B, Bruton PC, Saleeb RS, Arnedo M and others. SAF-A Regulates Interphase Chromosome Structure through Oligomerization with Chromatin-Associated RNAs. *Cell* 2017;169:1214-1227.e18.
18. Ernst J, Kellis M. Discovery and characterization of chromatin states for systematic annotation of the human genome. *Nat Biotechnol* 2010;28:817-25.
19. Ernst J, Kellis M. Chromatin-state discovery and genome annotation with ChromHMM. *Nat Protoc* 2017;12:2478-2492.
20. Cremer T, Cremer M, Hubner B, Strickfaden H, Smeets D, Popken J, Sterr M, Markaki Y, Rippe K, Cremer C. The 4D nucleome: Evidence for a dynamic nuclear landscape based on co-aligned active and inactive nuclear compartments. *FEBS Lett* 2015;589:2931-43.
21. Maeshima K, Ide S, Hibino K, Sasai M. Liquid-like behavior of chromatin. *Curr Opin Genet Dev* 2016;37:36-45.
22. Zhu P, Li G. Structural insights of nucleosome and the 30-nm chromatin fiber. *Curr Opin Struct Biol* 2016;36:106-15.
23. Robinson PJ, Rhodes D. Structure of the '30 nm' chromatin fibre: a key role for the linker histone. *Curr Opin Struct Biol* 2006;16:336-43.
24. Wu C, McGeehan JE, Travers A. A metastable structure for the compact 30-nm chromatin fibre. *FEBS Lett* 2016;590:935-42.
25. Voss TC, Hager GL. Visualizing chromatin dynamics in intact cells. *Biochim Biophys Acta* 2008;1783:2044-51.
26. Mateus A, Gordon LJ, Wayne GJ, Almqvist H, Axelsson H, Seashore-Ludlow B, Treyer A, Matsson P, Lundback T, West A and others. Prediction of intracellular exposure bridges the gap between target- and cell-based drug discovery. *Proc Natl Acad Sci U S A* 2017;114:E6231-e6239.
27. Evans ND, Errington RJ, Shelley M, Feeney GP, Chapman MJ, Godfrey KR, Smith PJ, Chappell MJ. A mathematical model for the in vitro kinetics of the anti-cancer agent topotecan. *Math Biosci* 2004;189:185-217.
28. Daddysman MK, Fecko CJ. Revisiting point FRAP to quantitatively characterize anomalous diffusion in live cells. *J Phys Chem B* 2013;117:1241-51.
29. Hauer MH, Gasser SM. Chromatin and nucleosome dynamics in DNA damage and repair. *Genes Dev* 2017;31:2204-2221.

30. Nair N, Shoaib M, Sorensen CS. Chromatin Dynamics in Genome Stability: Roles in Suppressing Endogenous DNA Damage and Facilitating DNA Repair. *Int J Mol Sci* 2017;18.
31. Wilson MD, Durocher D. Reading chromatin signatures after DNA double-strand breaks. *Philos Trans R Soc Lond B Biol Sci* 2017;372.
32. Uphoff S, Kapanidis AN. Studying the organization of DNA repair by single-cell and single-molecule imaging. *DNA Repair (Amst)* 2014;20:32-40.
33. Condie AG, Yan Y, Gerson SL, Wang Y. A Fluorescent Probe to Measure DNA Damage and Repair. *PLoS One* 2015;10:e0131330.
34. Toga T, Kuraoka I, Watanabe S, Nakano E, Takeuchi S, Nishigori C, Sugasawa K, Iwai S. Fluorescence detection of cellular nucleotide excision repair of damaged DNA. *Sci Rep* 2014;4:5578.
35. Fritz AJ, Ghule PN, Boyd JR, Tye CE, Page NA, Hong D, Shirley DJ, Weinheimer AS, Barutcu AR, Gerrard DL and others. Intranuclear and higher-order chromatin organization of the major histone gene cluster in breast cancer. *J Cell Physiol* 2018;233:1278-1290.
36. Ho L, Crabtree GR. Chromatin remodelling during development. *Nature* 2010;463:474-84.
37. Sequeira-Mendes J, Gutierrez C. Genome architecture: from linear organisation of chromatin to the 3D assembly in the nucleus. *Chromosoma* 2016;125:455-69.
38. Almassalha LM, Bauer GM, Wu W, Cherkezyan L, Zhang D, Kendra A, Gladstein S, Chandler JE, VanDerway D, Seagle B-LL and others. Macrogenomic engineering via modulation of the scaling of chromatin packing density. *Nature Biomedical Engineering* 2017;1:902-913.
39. Clapier CR, Iwasa J, Cairns BR, Peterson CL. Mechanisms of action and regulation of ATP-dependent chromatin-remodelling complexes. *Nat Rev Mol Cell Biol* 2017;18:407-422.
40. Pommier Y. Drugging topoisomerases: lessons and challenges. *ACS Chem Biol* 2013;8:82-95.
41. Pommier Y, Leo E, Zhang H, Marchand C. DNA topoisomerases and their poisoning by anticancer and antibacterial drugs. *Chem Biol* 2010;17:421-33.
42. Kinoshita K, Hirano T. Dynamic organization of mitotic chromosomes. *Curr Opin Cell Biol* 2017;46:46-53.
43. Galganski L, Urbanek MO, Krzyzosiak WJ. Nuclear speckles: molecular organization, biological function and role in disease. *Nucleic Acids Res* 2017;45:10350-10368.
44. Wali RK, Momi N, Dela Cruz M, Calderwood AH, Stypula-Cyrus Y, Almassalha L, Chhaparia A, Weber CR, Radosevich A, Tiwari AK and others. Higher Order Chromatin Modulator Cohesin SA1 Is an Early Biomarker for Colon Carcinogenesis: Race-Specific Implications. *Cancer Prev Res (Phila)* 2016;9:844-854.
45. Naughton C, Avlonitis N, Corless S, Prendergast JG, Mati IK, Eijk PP, Cockroft SL, Bradley M, Ylstra B, Gilbert N. Transcription forms and remodels supercoiling domains unfolding large-scale chromatin structures. *Nat Struct Mol Biol* 2013;20:387-95.
46. Muskhelishvili G, Travers A. The regulatory role of DNA supercoiling in nucleoprotein complex assembly and genetic activity. *Biophysical Reviews* 2016;8:5-22.

47. Smith PJ, Makinson TA. Cellular consequences of overproduction of DNA topoisomerase II in an ataxia-telangiectasia cell line. *Cancer Res* 1989;49:1118-24.
48. de Campos-Nebel M, Palmitelli M, Gonzalez-Cid M. A flow cytometry-based method for a high-throughput analysis of drug-stabilized topoisomerase II cleavage complexes in human cells. *Cytometry A* 2016;89:852-60.
49. Zhao H, Rybak P, Dobrucki J, Traganos F, Darzynkiewicz Z. Relationship of DNA damage signaling to DNA replication following treatment with DNA topoisomerase inhibitors camptothecin/topotecan, mitoxantrone, or etoposide. *Cytometry A* 2012;81:45-51.
50. Huang X, Traganos F, Darzynkiewicz Z. DNA damage induced by DNA topoisomerase I- and topoisomerase II-inhibitors detected by histone H2AX phosphorylation in relation to the cell cycle phase and apoptosis. *Cell Cycle* 2003;2:614-9.
51. Huang X, Okafuji M, Traganos F, Luther E, Holden E, Darzynkiewicz Z. Assessment of histone H2AX phosphorylation induced by DNA topoisomerase I and II inhibitors topotecan and mitoxantrone and by the DNA cross-linking agent cisplatin. *Cytometry A* 2004;58:99-110.
52. Smith PJ, Marquez N, Wiltshire M, Chappell S, Njoh K, Campbell L, Khan IA, Silvestre O, Errington RJ. Mitotic bypass via an occult cell cycle phase following DNA topoisomerase II inhibition in p53 functional human tumor cells. *Cell Cycle* 2007;6:2071-81.
53. Chang CC, Wang YR, Chen SF, Wu CC, Chan NL. New insights into DNA-binding by type IIA topoisomerases. *Curr Opin Struct Biol* 2013;23:125-33.
54. Fox ME, Smith PJ. Long-term inhibition of DNA synthesis and the persistence of trapped topoisomerase II complexes in determining the toxicity of the antitumor DNA intercalators mAMSA and mitoxantrone. *Cancer Res* 1990;50:5813-8.
55. Bollimpelli VS, Dholaniya PS, Kondapi AK. Topoisomerase IIbeta and its role in different biological contexts. *Arch Biochem Biophys* 2017;633:78-84.
56. Pang B, de Jong J, Qiao X, Wessels LF, Neefjes J. Chemical profiling of the genome with anti-cancer drugs defines target specificities. *Nat Chem Biol* 2015;11:472-80.
57. Errington RJ, Ameer-Beg SM, Vojnovic B, Patterson LH, Zloh M, Smith PJ. Advanced microscopy solutions for monitoring the kinetics and dynamics of drug-DNA targeting in living cells. *Adv Drug Deliv Rev* 2005;57:153-67.
58. Waldes H, Center MS. Adriamycin-induced compaction of isolated chromatin. *Biochem Pharmacol* 1982;31:1057-61.
59. Zunino F, Di Marco A, Zaccara A, Gambetta RA. The interaction of daunorubicin and doxorubicin with DNA and chromatin. *Biochim Biophys Acta* 1980;607:206-14.
60. Rabbani A, Finn RM, Ausio J. The anthracycline antibiotics: antitumor drugs that alter chromatin structure. *Bioessays* 2005;27:50-6.
61. Yang F, Teves SS, Kemp CJ, Henikoff S. Doxorubicin, DNA torsion, and chromatin dynamics. *Biochimica et biophysica acta* 2014;1845:84-89.
62. Pang B, Qiao X, Janssen L, Velds A, Groothuis T, Kerkhoven R, Nieuwland M, Ovaa H, Rottenberg S, van Tellingen O and others. Drug-induced histone eviction from open

- chromatin contributes to the chemotherapeutic effects of doxorubicin. *Nat Commun* 2013;4:1908.
63. Krishan A, Hamelik RM. Flow cytometric monitoring of fluorescent drug retention and efflux. *Methods Mol Med* 2005;111:149-66.
 64. Krishan A, Ganapathi R. Laser flow cytometry and cancer chemotherapy: detection of intracellular anthracyclines by flow cytometry. *J Histochem Cytochem* 1979;27:1655-6.
 65. Nienhaus K, Nienhaus GU. Where Do We Stand with Super-Resolution Optical Microscopy? *J Mol Biol* 2016;428:308-322.
 66. Matsuda A, Shao L, Boulanger J, Kervrann C, Carlton PM, Kner P, Agard D, Sedat JW. Condensed mitotic chromosome structure at nanometer resolution using PALM and EGFP-histones. *PLoS One* 2010;5:e12768.
 67. Smeets D, Markaki Y, Schmid VJ, Kraus F, Tattermusch A, Cerase A, Sterr M, Fiedler S, Demmerle J, Popken J and others. Three-dimensional super-resolution microscopy of the inactive X chromosome territory reveals a collapse of its active nuclear compartment harboring distinct Xist RNA foci. *Epigenetics Chromatin* 2014;7:8.
 68. Zessin PJ, Finan K, Heilemann M. Super-resolution fluorescence imaging of chromosomal DNA. *J Struct Biol* 2012;177:344-8.
 69. Ricci MA, Manzo C, Garcia-Parajo MF, Lakadamyali M, Cosma MP. Chromatin fibers are formed by heterogeneous groups of nucleosomes in vivo. *Cell* 2015;160:1145-58.
 70. Boettiger AN, Bintu B, Moffitt JR, Wang S, Beliveau BJ, Fudenberg G, Imakaev M, Mirny LA, Wu CT, Zhuang X. Super-resolution imaging reveals distinct chromatin folding for different epigenetic states. *Nature* 2016;529:418-22.
 71. Szczurek A, Klewes L, Xing J, Gourram A, Birk U, Knecht H, Dobrucki JW, Mai S, Cremer C. Imaging chromatin nanostructure with binding-activated localization microscopy based on DNA structure fluctuations. *Nucleic Acids Res* 2017;45:e56.
 72. Szczurek A, Xing J, Birk UJ, Cremer C. Single Molecule Localization Microscopy of Mammalian Cell Nuclei on the Nanoscale. *Front Genet* 2016;7:114.
 73. Szczurek AT, Prakash K, Lee HK, Zurek-Biesiada DJ, Best G, Hagmann M, Dobrucki JW, Cremer C, Birk U. Single molecule localization microscopy of the distribution of chromatin using Hoechst and DAPI fluorescent probes. *Nucleus* 2014;5:331-40.
 74. Zurek-Biesiada D, Szczurek AT, Prakash K, Mohana GK, Lee HK, Roignant JY, Birk UJ, Dobrucki JW, Cremer C. Localization microscopy of DNA in situ using Vybrant((R)) DyeCycle Violet fluorescent probe: A new approach to study nuclear nanostructure at single molecule resolution. *Exp Cell Res* 2016;343:97-106.
 75. Cremer C, Szczurek A, Schock F, Gourram A, Birk U. Super-resolution microscopy approaches to nuclear nanostructure imaging. *Methods* 2017;123:11-32.
 76. Dong B, Almassalha LM, Soetikno BT, Chandler JE, Nguyen TQ, Urban BE, Sun C, Zhang HF, Backman V. Stochastic fluorescence switching of nucleic acids under visible light illumination. *Opt Express* 2017;25:7929-7944.

77. Ou HD, Phan S, Deerinck TJ, Thor A, Ellisman MH, O'Shea CC. ChromEMT: Visualizing 3D chromatin structure and compaction in interphase and mitotic cells. *Science* 2017;357.
78. Malatesta M, Pellicciari C, Cisterna B, Costanzo M, Galimberti V, Biggiogera M, Zancanaro C. Tracing nanoparticles and photosensitizing molecules at transmission electron microscopy by diaminobenzidine photo-oxidation. *Micron* 2014;59:44-51.
79. Crissman HA, Orlicky DJ, Kissane RJ. Fluorescent DNA probes for flow cytometry. Considerations and prospects. *J Histochem Cytochem* 1979;27:1652-4.
80. Latt SA. Microfluorometric detection of deoxyribonucleic acid replication in human metaphase chromosomes. *Proc Natl Acad Sci U S A* 1973;70:3395-9.
81. Lukinavicius G, Blaukopf C, Pershagen E, Schena A, Reymond L, Derivery E, Gonzalez-Gaitan M, D'Este E, Hell SW, Gerlich DW and others. SiR-Hoechst is a far-red DNA stain for live-cell nanoscopy. *Nat Commun* 2015;6:8497.
82. Huang WC, Lee CY, Hsieh TS. Single-molecule Forster resonance energy transfer (FRET) analysis discloses the dynamics of the DNA-topoisomerase II (Top2) interaction in the presence of TOP2-targeting agents. *J Biol Chem* 2017;292:12589-12598.
83. Zhao H, Oczos J, Janowski P, Trembecka D, Dobrucki J, Darzynkiewicz Z, Wlodkowic D. Rationale for the real-time and dynamic cell death assays using propidium iodide. *Cytometry A* 2010;77:399-405.
84. Park CH, Kimler BF, Smith TK. Comparison of the supravital DNA dyes Hoechst 33342 and DAPI for flow cytometry and clonogenicity studies of human leukemic marrow cells. *Exp Hematol* 1985;13:1039-43.
85. Akagi J, Kordon M, Zhao H, Matuszek A, Dobrucki J, Errington R, Smith PJ, Takeda K, Darzynkiewicz Z, Wlodkowic D. Real-time cell viability assays using a new anthracycline derivative DRAQ7(R). *Cytometry A* 2013;83:227-34.
86. Smith PJ, Furon E, Wiltshire M, Chappell S, Patterson LH, Shnyder SD, Falconer RA, Errington RJ. NCAM polysialylation during adherence transitions: live cell monitoring using an antibody-mimetic EGFP-endosialidase and the viability dye DRAQ7. *Cytometry A* 2013;83:659-71.
87. Purschke M, Rubio N, Held KD, Redmond RW. Phototoxicity of Hoechst 33342 in time-lapse fluorescence microscopy. *Photochem Photobiol Sci* 2010;9:1634-9.
88. Wlodkowic D, Darzynkiewicz Z. Please do not disturb: destruction of chromatin structure by supravital nucleic acid probes revealed by a novel assay of DNA-histone interaction. *Cytometry A* 2008;73:877-9.
89. Wojcik K, Dobrucki JW. Interaction of a DNA intercalator DRAQ5, and a minor groove binder SYTO17, with chromatin in live cells--influence on chromatin organization and histone-DNA interactions. *Cytometry A* 2008;73:555-62.
90. Zhao H, Traganos F, Dobrucki J, Wlodkowic D, Darzynkiewicz Z. Induction of DNA damage response by the supravital probes of nucleic acids. *Cytometry A* 2009;75:510-9.

91. Smith PJ, Furon E, Wiltshire M, Campbell L, Feeney GP, Snyder RD, Errington RJ. ABCG2-associated resistance to Hoechst 33342 and topotecan in a murine cell model with constitutive expression of side population characteristics. *Cytometry A* 2009;75:924-33.
92. Zhu H, Cheng P, Chen P, Pu K. Recent progress in the development of near-infrared organic photothermal and photodynamic nanotherapeutics. *Biomater Sci* 2018;6:746-765.
93. Rigler R, Killander D, Bolund L, Ringertz NR. Cytochemical characterization of deoxyribonucleoprotein in individual cell nuclei. Techniques for obtaining heat denaturation curves with the aid of acridine orange microfluorimetry and ultraviolet microspectrophotometry. *Exp Cell Res* 1969;55:215-24.
94. Darzynkiewicz Z, Traganos F, Andreeff M, Sharpless T, Melamed MR. Different sensitivity of chromatin to acid denaturation in quiescent and cycling cells as revealed by flow cytometry. *J Histochem Cytochem* 1979;27:478-85.
95. Darzynkiewicz Z, Traganos F, Melamed MR. New cell cycle compartments identified by multiparameter flow cytometry. *Cytometry* 1980;1:98-108.
96. Frisa PS, Jacobberger JW. Cytometry of chromatin bound Mcm6 and PCNA identifies two states in G1 that are separated functionally by the G1 restriction point. *BMC Cell Biol* 2010;11:26.
97. Behbehani GK, Bendall SC, Clutter MR, Fantl WJ, Nolan GP. Single-cell mass cytometry adapted to measurements of the cell cycle. *Cytometry A* 2012;81:552-66.
98. Griesdoorn V, Brown MR, Wiltshire M, Smith PJ, Errington RJ. Tracking the Cyclin B1-GFP Sensor to Profile the Pattern of Mitosis Versus Mitotic Bypass. *Methods Mol Biol* 2016;1342:279-85.
99. Matsubara T, Nakagome Y. High-resolution banding by treating cells with acridine orange before fixation. *Cytogenet Cell Genet* 1983;35:148-51.
100. Caspersson T, Zech L, Johansson C, Modest EJ. Identification of human chromosomes by DNA-binding fluorescent agents. *Chromosoma* 1970;30:215-27.
101. Evenson DP, Darzynkiewicz Z, Melamed MR. Relation of mammalian sperm chromatin heterogeneity to fertility. *Science* 1980;210:1131-3.
102. Evenson DP. Sperm chromatin structure assay (SCSA(R)). *Methods Mol Biol* 2013;927:147-64.
103. Gorczyca W, Traganos F, Jesionowska H, Darzynkiewicz Z. Presence of DNA strand breaks and increased sensitivity of DNA in situ to denaturation in abnormal human sperm cells: analogy to apoptosis of somatic cells. *Exp Cell Res* 1993;207:202-5.
104. Dobrucki J, Darzynkiewicz Z. Chromatin condensation and sensitivity of DNA in situ to denaturation during cell cycle and apoptosis--a confocal microscopy study. *Micron* 2001;32:645-52.
105. Evenson DP, Jost LK, Marshall D, Zinaman MJ, Clegg E, Purvis K, de Angelis P, Claussen OP. Utility of the sperm chromatin structure assay as a diagnostic and prognostic tool in the human fertility clinic. *Hum Reprod* 1999;14:1039-49.

106. Evenson DP, Larson KL, Jost LK. Sperm chromatin structure assay: its clinical use for detecting sperm DNA fragmentation in male infertility and comparisons with other techniques. *J Androl* 2002;23:25-43.
107. Traganos F, Darzynkiewicz Z. Lysosomal proton pump activity: supravital cell staining with acridine orange differentiates leukocyte subpopulations. *Methods Cell Biol* 1994;41:185-94.
108. Pierzynska-Mach A, Janowski PA, Dobrucki JW. Evaluation of acridine orange, LysoTracker Red, and quinacrine as fluorescent probes for long-term tracking of acidic vesicles. *Cytometry A* 2014;85:729-37.
109. Chang Q, Ornatsky OI, Koch CJ, Chaudary N, Marie-Egyptienne DT, Hill RP, Tanner SD, Hedley DW. Single-cell measurement of the uptake, intratumoral distribution and cell cycle effects of cisplatin using mass cytometry. *Int J Cancer* 2015;136:1202-9.
110. Mei HE, Leipold MD, Maecker HT. Platinum-conjugated antibodies for application in mass cytometry. *Cytometry A* 2016;89:292-300.
111. Fienberg HG, Simonds EF, Fantl WJ, Nolan GP, Bodenmiller B. A platinum-based covalent viability reagent for single-cell mass cytometry. *Cytometry A* 2012;81:467-75.
112. Breuzard G, Piot O, Angiboust JF, Manfait M, Candeil L, Del Rio M, Millot JM. Changes in adsorption and permeability of mitoxantrone on plasma membrane of BCRP/MXR resistant cells. *Biochem Biophys Res Commun* 2005;329:64-70.
113. Nolan JP, Sebba DS. Surface-enhanced Raman scattering (SERS) cytometry. *Methods Cell Biol* 2011;102:515-32.
114. Mattheus C, Boydston-White S, Miljkovic M, Romeo M, Diem M. Raman and infrared microspectral imaging of mitotic cells. *Appl Spectrosc* 2006;60:1-8.
115. Lu FK, Basu S, Igras V, Hoang MP, Ji M, Fu D, Holtom GR, Neel VA, Freudiger CW, Fisher DE and others. Label-free DNA imaging in vivo with stimulated Raman scattering microscopy. *Proc Natl Acad Sci U S A* 2015;112:11624-9.
116. Zhang X, Roeffaers MB, Basu S, Daniele JR, Fu D, Freudiger CW, Holtom GR, Xie XS. Label-free live-cell imaging of nucleic acids using stimulated Raman scattering microscopy. *Chemphyschem* 2012;13:1054-9.
117. Di Napoli C, Pope I, Masia F, Watson P, Langbein W, Borri P. Hyperspectral and differential CARS microscopy for quantitative chemical imaging in human adipocytes. *Biomed Opt Express* 2014;5:1378-90.
118. Karuna A, Masia F, Borri P, Langbein W. Hyperspectral volumetric coherent anti-Stokes Raman scattering microscopy: quantitative volume determination and NaCl as non-resonant standard. *J Raman Spectrosc* 2016;47:1167-1173.
119. Giordano S, Morosi L, Veglianesi P, Licandro SA, Frapolli R, Zucchetti M, Cappelletti G, Falcicola L, Pifferi V, Visentin S and others. 3D Mass Spectrometry Imaging Reveals a Very Heterogeneous Drug Distribution in Tumors. *Sci Rep* 2016;6:37027.
120. Lahiri S, Sun N, Buck A, Imhof A, Walch A. MALDI imaging mass spectrometry as a novel tool for detecting histone modifications in clinical tissue samples. *Expert Rev Proteomics* 2016;13:275-84.

121. Almassalha LM, Bauer GM, Chandler JE, Gladstein S, Cherkezyan L, Stypula-Cyrus Y, Weinberg S, Zhang D, Thusgaard Ruhoff P, Roy HK and others. Label-free imaging of the native, living cellular nanoarchitecture using partial-wave spectroscopic microscopy. *Proc Natl Acad Sci U S A* 2016;113:E6372-e6381.
122. Li Y, Almassalha LM, Chandler JE, Zhou X, Stypula-Cyrus YE, Hujsak KA, Roth EW, Bleher R, Subramanian H, Szleifer I and others. The effects of chemical fixation on the cellular nanostructure. *Exp Cell Res* 2017;358:253-259.
123. Chandler JE, Stypula-Cyrus Y, Almassalha L, Bauer G, Bowen L, Subramanian H, Szleifer I, Backman V. Colocalization of cellular nanostructure using confocal fluorescence and partial wave spectroscopy. *J Biophotonics* 2017;10:377-384.
124. Smith PJ, Blunt N, Wiltshire M, Hoy T, Teesdale-Spittle P, Craven MR, Watson JV, Amos WB, Errington RJ, Patterson LH. Characteristics of a novel deep red/infrared fluorescent cell-permeant DNA probe, DRAQ5, in intact human cells analyzed by flow cytometry, confocal and multiphoton microscopy. *Cytometry* 2000;40:280-91.
125. Njoh KL, Patterson LH, Zloh M, Wiltshire M, Fisher J, Chappell S, Ameer-Beg S, Bai Y, Matthews D, Errington RJ and others. Spectral analysis of the DNA targeting bisalkylaminoanthraquinone DRAQ5 in intact living cells. *Cytometry A* 2006;69:805-14.
126. Moore MJ, Strohm EM, Kolios MC. Evaluation of the morphological parameters of cancer cells using high-frequency ultrasound and photoacoustics. 2015 21-24 Oct. 2015. p 1-4.
127. Wlodkowic D, Telford W, Skommer J, Darzynkiewicz Z. Apoptosis and beyond: cytometry in studies of programmed cell death. *Methods Cell Biol* 2011;103:55-98.
128. Chan LL, McCulley KJ, Kessel SL. Assessment of Cell Viability with Single-, Dual-, and Multi-Staining Methods Using Image Cytometry. *Methods Mol Biol* 2017;1601:27-41.
129. Halicka HD, Bedner E, Darzynkiewicz Z. Segregation of RNA and separate packaging of DNA and RNA in apoptotic bodies during apoptosis. *Exp Cell Res* 2000;260:248-56.
130. Thierry AR, El Messaoudi S, Gahan PB, Anker P, Stroun M. Origins, structures, and functions of circulating DNA in oncology. *Cancer Metastasis Rev* 2016;35:347-76.
131. Dolman NJ, Chambers KM, Mandavilli B, Batchelor RH, Janes MS. Tools and techniques to measure mitophagy using fluorescence microscopy. *Autophagy* 2013;9:1653-62.
132. Warnes G. Flow cytometric assays for the study of autophagy. *Methods* 2015;82:21-8.
133. Ghavami S, Shojaei S, Yeganeh B, Ande SR, Jangamreddy JR, Mehrpour M, Christoffersson J, Chaabane W, Moghadam AR, Kashani HH and others. Autophagy and apoptosis dysfunction in neurodegenerative disorders. *Prog Neurobiol* 2014;112:24-49.
134. Li M, Gao P, Zhang J. Crosstalk between Autophagy and Apoptosis: Potential and Emerging Therapeutic Targets for Cardiac Diseases. *Int J Mol Sci* 2016;17:332.
135. Fullgrabe J, Heldring N, Hermanson O, Joseph B. Cracking the survival code: autophagy-related histone modifications. *Autophagy* 2014;10:556-61.

136. Fuchs TA, Abed U, Goosmann C, Hurwitz R, Schulze I, Wahn V, Weinrauch Y, Brinkmann V, Zychlinsky A. Novel cell death program leads to neutrophil extracellular traps. *J Cell Biol* 2007;176:231-41.
137. Brinkmann V, Reichard U, Goosmann C, Fauler B, Uhlemann Y, Weiss DS, Weinrauch Y, Zychlinsky A. Neutrophil extracellular traps kill bacteria. *Science* 2004;303:1532-5.
138. Germic N, Stojkov D, Oberson K, Yousefi S, Simon HU. Neither eosinophils nor neutrophils require ATG5-dependent autophagy for extracellular DNA trap formation. *Immunology* 2017;152:517-525.
139. Xu F, Zhang C, Zou Z, Fan EKY, Chen L, Li Y, Billiar TR, Wilson MA, Shi X, Fan J. Aging-related Atg5 defect impairs neutrophil extracellular traps formation. *Immunology* 2017;151:417-432.
140. Delgado-Rizo V, Martínez-Guzmán MA, Iñiguez-Gutierrez L, García-Orozco A, Alvarado-Navarro A, Fafutis-Morris M. Neutrophil Extracellular Traps and Its Implications in Inflammation: An Overview. *Frontiers in Immunology* 2017;8:81.
141. Yousefi S, Simon HU. NETosis - Does It Really Represent Nature's "Suicide Bomber"? *Front Immunol* 2016;7:328.
142. Lee SR, Han J. Mitochondrial Nucleoid: Shield and Switch of the Mitochondrial Genome. *Oxid Med Cell Longev* 2017;2017:8060949.
143. Soderberg D, Segelmark M. Neutrophil extracellular traps in vasculitis, friend or foe? *Curr Opin Rheumatol* 2018;30:16-23.
144. Agraz-Cibrian JM, Giraldo DM, Mary FM, Urcuqui-Inchima S. Understanding the molecular mechanisms of NETs and their role in antiviral innate immunity. *Virus Res* 2017;228:124-133.
145. Brinkmann V, Laube B, Abu Abed U, Goosmann C, Zychlinsky A. Neutrophil Extracellular Traps: How to Generate and Visualize Them. *Journal of Visualized Experiments : JoVE* 2010:1724.
146. Mohanty T, Sorensen OE, Nordenfelt P. NETQUANT: Automated Quantification of Neutrophil Extracellular Traps. *Front Immunol* 2017;8:1999.
147. Carmona-Rivera C, Kaplan MJ. Induction and Quantification of NETosis. *Curr Protoc Immunol* 2016;115:14.41.1-14.41.14.
148. Masuda S, Shimizu S, Matsuo J, Nishibata Y, Kusunoki Y, Hattanda F, Shida H, Nakazawa D, Tomaru U, Atsumi T and others. Measurement of NET formation in vitro and in vivo by flow cytometry. *Cytometry A* 2017;91:822-829.
149. Gavillet M, Martinod K, Renella R, Harris C, Shapiro NI, Wagner DD, Williams DA. Flow cytometric assay for direct quantification of Neutrophil Extracellular Traps in blood samples. *American journal of hematology* 2015;90:1155-1158.
150. Kenny EF, Herzig A, Krüger R, Muth A, Mondal S, Thompson PR, Brinkmann V, von Bernuth H, Zychlinsky A. Diverse stimuli engage different neutrophil extracellular trap pathways. *eLife* 2017;6:e24437.

151. Okubo K, Kamiya M, Urano Y, Nishi H, Herter JM, Mayadas T, Hirohama D, Suzuki K, Kawakami H, Tanaka M and others. Lactoferrin Suppresses Neutrophil Extracellular Traps Release in Inflammation. *EBioMedicine* 2016;10:204-15.
152. Urban CF, Reichard U, Brinkmann V, Zychlinsky A. Neutrophil extracellular traps capture and kill *Candida albicans* yeast and hyphal forms. *Cell Microbiol* 2006;8:668-76.
153. Ginley BG, Emmons T, Lutnick B, Urban CF, Segal BH, Sarder P. Computational detection and quantification of human and mouse neutrophil extracellular traps in flow cytometry and confocal microscopy. *Sci Rep* 2017;7:17755.
154. Smith P. Cytomics of the tumour microenvironment: therapeutic targeting (keynote lecture). *Journal of Inflammation (London, England)* 2015;12:O10-O10.
155. Patterson LH, Murray GI. Tumour cytochrome P450 and drug activation. *Curr Pharm Des* 2002;8:1335-47.
156. Smith PJ, Desnoyers R, Blunt N, Giles Y, Patterson LH, Watson JV. Flow cytometric analysis and confocal imaging of anticancer alkylaminoanthraquinones and their N-oxides in intact human cells using 647-nm krypton laser excitation. *Cytometry* 1997;27:43-53.
157. Phillips RM. Targeting the hypoxic fraction of tumours using hypoxia-activated prodrugs. *Cancer Chemother Pharmacol* 2016;77:441-57.
158. Smith PJ, Griesdoorn V, Silvestre OF, Errington RJ. Microenvironment Cytometry. In: Robinson JP, Cossarizza A, editors. *Single Cell Analysis: Contemporary Research and Clinical Applications*. Singapore: Springer Singapore; 2017. p 1-38.
159. Darzynkiewicz Z, Traganos F, Zhao H, Halicka HD, Skommer J, Wlodkowic D. Analysis of individual molecular events of DNA damage response by flow- and image-assisted cytometry. *Methods Cell Biol* 2011;103:115-47.
160. Chen AY, Yu C, Bodley A, Peng LF, Liu LF. A new mammalian DNA topoisomerase I poison Hoechst 33342: cytotoxicity and drug resistance in human cell cultures. *Cancer Res* 1993;53:1332-7.
161. Smith PJ, Wiltshire M, Chappell SC, Cosentino L, Burns PA, Pors K, Errington RJ. Kinetic analysis of intracellular Hoechst 33342--DNA interactions by flow cytometry: misinterpretation of side population status? *Cytometry A* 2013;83:161-9.
162. Andersson BS, Beran M, Barlogie B, Van NT, McCredie KB. Analysis of nuclear m-AMSA content by DNA fluorochrome competition. *Eur J Cancer Clin Oncol* 1986;22:883-9.
163. Preisler HD. Alteration of binding of the supravital dye Hoechst 33342 to human leukemic cells by adriamycin. *Cancer Treat Rep* 1978;62:1393-6.
164. Breuzard G, Angiboust JF, Jeannesson P, Manfait M, Millot JM. Surface-enhanced Raman scattering reveals adsorption of mitoxantrone on plasma membrane of living cells. *Biochem Biophys Res Commun* 2004;320:615-21.
165. Khan SN, Yennamalli R, Subbarao N, Khan AU. Mitoxantrone induced impediment of histone acetylation and structural flexibility of the protein. *Cell Biochem Biophys* 2011;60:209-18.

166. Bartkowiak J, Kapuscinski J, Melamed MR, Darzynkiewicz Z. Selective displacement of nuclear proteins by antitumor drugs having affinity for nucleic acids. *Proc Natl Acad Sci U S A* 1989;86:5151-4.
167. Smith PJ, Morgan SA, Fox ME, Watson JV. Mitoxantrone-DNA binding and the induction of topoisomerase II associated DNA damage in multi-drug resistant small cell lung cancer cells. *Biochem Pharmacol* 1990;40:2069-78.
168. Goodell MA, Brose K, Paradis G, Conner AS, Mulligan RC. Isolation and functional properties of murine hematopoietic stem cells that are replicating in vivo. *J Exp Med* 1996;183:1797-806.
169. Smith PJ, Nakeff A, Watson JV. Flow-cytometric detection of changes in the fluorescence emission spectrum of a vital DNA-specific dye in human tumour cells. *Exp Cell Res* 1985;159:37-46.
170. Watson JV, Nakeff A, Chambers SH, Smith PJ. Flow cytometric fluorescence emission spectrum analysis of Hoechst-33342-stained DNA in chicken thymocytes. *Cytometry* 1985;6:310-5.
171. Krishan A. Effect of drug efflux blockers on vital staining of cellular DNA with Hoechst 33342. *Cytometry* 1987;8:642-5.
172. Morgan SA, Watson JV, Twentyman PR, Smith PJ. Flow cytometric analysis of Hoechst 33342 uptake as an indicator of multi-drug resistance in human lung cancer. *Br J Cancer* 1989;60:282-7.
173. Petriz J. Flow cytometry of the side population (SP). *Curr Protoc Cytom* 2013;Chapter 9:Unit9.23.
174. Chappell MJ, Evans ND, Errington RJ, Khan IA, Campbell L, Ali R, Godfrey KR, Smith PJ. A coupled drug kinetics-cell cycle model to analyse the response of human cells to intervention by topotecan. *Comput Methods Programs Biomed* 2008;89:169-78.
175. Atari MI, Chappell MJ, Errington RJ, Smith PJ, Evans ND. Kinetic modelling of the role of the aldehyde dehydrogenase enzyme and the breast cancer resistance protein in drug resistance and transport. *Comput Methods Programs Biomed* 2011;104:93-103.
176. Garralda E, Dienstmann R, Tabernero J. Pharmacokinetic/Pharmacodynamic Modeling for Drug Development in Oncology. *Am Soc Clin Oncol Educ Book* 2017;37:210-215.
177. Kim S, Thiessen PA, Bolton EE, Chen J, Fu G, Gindulyte A, Han L, He J, He S, Shoemaker BA and others. PubChem Substance and Compound databases. *Nucleic Acids Res* 2016;44:D1202-13.
178. Patterson LH. Rationale for the use of aliphatic N-oxides of cytotoxic anthraquinones as prodrug DNA binding agents: a new class of bioreductive agent. *Cancer Metastasis Rev* 1993;12:119-34.
179. Patterson LH. Bioreductively activated antitumor N-oxides: the case of AQ4N, a unique approach to hypoxia-activated cancer chemotherapy. *Drug Metab Rev* 2002;34:581-92.
180. Nesbitt H, Byrne NM, Williams SN, Ming L, Worthington J, Errington RJ, Patterson LH, Smith PJ, McKeown SR, McKenna DJ. Targeting Hypoxic Prostate Tumors Using the Novel Hypoxia-

- Activated Prodrug OCT1002 Inhibits Expression of Genes Associated with Malignant Progression. *Clin Cancer Res* 2017;23:1797-1808.
181. Nesbitt H, Worthington J, Errington RJ, Patterson LH, Smith PJ, McKeown SR, McKenna DJ. The unidirectional hypoxia-activated prodrug OCT1002 inhibits growth and vascular development in castrate-resistant prostate tumors. *Prostate* 2017;77:1539-1547.
 182. Tredan O, Garbens AB, Lalani AS, Tannock IF. The hypoxia-activated ProDrug AQ4N penetrates deeply in tumor tissues and complements the limited distribution of mitoxantrone. *Cancer Res* 2009;69:940-7.
 183. Kapuscinski J, Darzynkiewicz Z. Relationship between the pharmacological activity of antitumor drugs Ametantrone and mitoxantrone (Novatrone) and their ability to condense nucleic acids. *Proc Natl Acad Sci U S A* 1986;83:6302-6.
 184. Bell DH. Characterization of the fluorescence of the antitumor agent, mitoxantrone. *Biochim Biophys Acta* 1988;949:132-7.
 185. Fox ME, Smith PJ. Subcellular localisation of the antitumour drug mitoxantrone and the induction of DNA damage in resistant and sensitive human colon carcinoma cells. *Cancer Chemother Pharmacol* 1995;35:403-10.
 186. Elfer KN, Sholl AB, Wang M, Tulman DB, Mandava SH, Lee BR, Brown JQ. DRAQ5 and Eosin ('D&E') as an Analog to Hematoxylin and Eosin for Rapid Fluorescence Histology of Fresh Tissues. *PLoS One* 2016;11:e0165530.
 187. Smith PJ, Wiltshire M, Errington RJ. DRAQ5 labeling of nuclear DNA in live and fixed cells. *Curr Protoc Cytom* 2004;Chapter 7:Unit 7.25.
 188. McGrath KE, Bushnell TP, Palis J. Multispectral imaging of hematopoietic cells: where flow meets morphology. *J Immunol Methods* 2008;336:91-7.
 189. Kudryavtsev I, Serebryakova M, Solovjeva L, Svetlova M, Firsanov D. Rapid Detection of Apoptosis in Cultured Mammalian Cells. *Methods Mol Biol* 2017;1644:105-111.
 190. Pan Y, Kaatz L. Use of image-based flow cytometry in bacterial viability analysis using fluorescent probes. *Curr Protoc Microbiol* 2012;Chapter 2:Unit 2C.5.
 191. Wlodkowic D, Akagi J, Dobrucki J, Errington R, Smith PJ, Takeda K, Darzynkiewicz Z. Kinetic viability assays using DRAQ7 probe. *Curr Protoc Cytom* 2013;Chapter 9:Unit 9.41.
 192. Pieper IL, Radley G, Chan CH, Friedmann Y, Foster G, Thornton CA. Quantification methods for human and large animal leukocytes using DNA dyes by flow cytometry. *Cytometry A* 2016;89:565-74.
 193. Martin RM, Leonhardt H, Cardoso MC. DNA labeling in living cells. *Cytometry A* 2005;67:45-52.
 194. Titford M. The long history of hematoxylin. *Biotech Histochem* 2005;80:73-8.
 195. Biran A, Meshorer E. Concise review: chromatin and genome organization in reprogramming. *Stem Cells* 2012;30:1793-9.
 196. Gaspar-Maia A, Alajem A, Meshorer E, Ramalho-Santos M. Open chromatin in pluripotency and reprogramming. *Nat Rev Mol Cell Biol* 2011;12:36-47.

